

# A Novel Double-Exposure Shadowgraph Method for Observation of Optodynamic Shock Waves Using Fiber-Optic Illumination

Tadej Perhavec<sup>1,2,\*</sup> - Janez Diaci<sup>1</sup>

<sup>1</sup> University of Ljubljana, Faculty of Mechanical Engineering, Slovenia

<sup>2</sup> Fotona d.d., Slovenia

*A novel double-exposure shadowgraph method is presented which allows visualization of an expanding shock wave in two time instances on a single image. The method has been developed to study shock waves generated in air during interaction of Er:YAG laser light with water and biological tissues. The shock wave is illuminated by pulsed green laser light coupled into two optical fibers of different lengths to establish two illumination flashes separated by a fixed time delay. An image of the shock wave region, acquired by a digital still camera, exhibits two well separated shock wavefronts. The optical set-up is analyzed using a paraxial ray model to explain the observed eccentricity of the two acquired wavefronts and provide guidelines for assembling the set-up.*

©2010 Journal of Mechanical Engineering. All rights reserved.

**Keywords:** shadowgraph, laser ablation, shock propagation

## 0 INTRODUCTION

Erbium lasers are well established in medicine and surgery [1] and [2]. They emit pulsed light at wavelengths where water as the main organic tissue component is highly absorptive [2]. During ablative laser-tissue interaction micro explosions occur which produce shock waves that propagate into the tissue and into the surrounding air. As they contain important information about the interaction processes they have been the object of many recent studies. For example, acoustic energy is a suitable parameter for the discrimination between necrotic and vital tissue subjected to Er:YAG laser ablation [3]. The methods used in the characterization of shock waves in air include microphone measurements [3] and [4] and different optical techniques, such as schlieren and shadowgraphy [3], [5] and [6], beam deflection probe [8], interferometry [8] and [9] and holographic recording [10]. Since the ablative shocks are short transient wave phenomena which exhibit significant pulse to pulse variations there is a special interest in methods that provide spatially and temporally resolved characterization of the shocks. Multiple-pass laser beam-deflection probe [11] for example can provide temporally resolved detection in a limited number of points in space while high-speed

cinematography [12] is capable of capturing spatially resolved information (holograms) in a limited number of time instances.

This article presents a double-exposure shadowgraph method which allows acquisition of a high-resolution image that exhibits an expanding shock wavefront (WF) in two time instances. A frequency doubled Q-switched Nd:YAG laser is used for illumination. Its output light is coupled into two optical fibers of different lengths to obtain two short light flashes which are separated by a fixed time delay. In the experiments to develop this method we studied shock waves in air which were generated during interaction of Er:YAG laser light with water. Water has been used here rather than tissue to have homogeneous interaction and propagation media with well known physical properties and predictable geometry. This facilitates comparison between the experimental data and theoretical results.

## 1 EXPERIMENT

A schematic of the experimental set-up is shown in Fig. 1. A free-running Er:YAG laser system (Fotona Fidelis Plus III, designed for dental applications) with 2.94  $\mu\text{m}$  wavelength, is used as the ablation source emitting pulses with 1.5  $\mu\text{s}$  duration, and 1.9 mJ energy. Its output

\*Corr. Author's Address: Fotona d.d., Stegne 7, SI – 1210 Ljubljana, Slovenia, tadej.perhavec@fotona.com

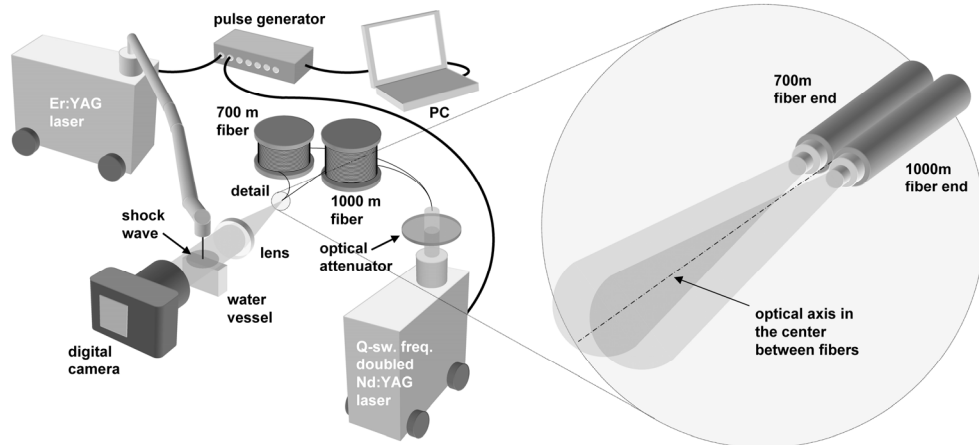


Fig. 1. Experiment set-up of the shadowgraph photography with a detailed view of fiber end tips

beam is guided through an articulated arm and focused to a diameter of 0.9 mm on the free surface of deionized water standing in a glass vessel. A frequency doubled (532 nm wavelength) Q-switched Nd:YAG laser system (Fotona QX, Slovenia) is used as the illumination source. Emitted pulses with duration and energy 6 ns and 300 mJ, respectively, are attenuated using neutral density filter and coupled directly into 700 m and 1000 m long multimode communication fibers with core diameters of 63  $\mu\text{m}$ .

Fibers of considerable length are used to achieve speckle-free illumination as previously described in similar experiments [3] and [5]. Several factors are considered to determine the difference of fiber lengths: propagation speed in communication fibers, expected shock wave propagation speed, magnification of the imaging system and size of the imaging sensor. The difference of fiber lengths influences the spatial separation and contrast of the two WFs on the image. The selected length difference of 300 m, which gives rise to a 1.563  $\mu\text{s}$  time delay between the illumination pulses, has proved to be adequate for our application (study of weak ablative shocks in air). If any of the above parameters significantly changes, e.g. when studying shock wave propagation in water, the fiber lengths need to be properly adjusted. The fiber ends are positioned at the focus of a converging lens (57 mm focal length), aligned horizontally and parallel to each other and to the optical axis of the lens to obtain collimated horizontal illuminating beams. The optical axis is placed approximately at the free water surface. The ablation beam axis intersects the optical axis of the imaging set-up

and is perpendicular to it and to the free water surface.

A simplified top-view schematic of the optical set-up is shown in Fig. 2 with lateral dimensions greatly exaggerated for clarity. The actual distance between the fibers was  $D = 0.19$  mm.

The water vessel is placed between the lens and a digital camera (Canon EOS 300D) which collects the illumination beams that pass through the shock wave. The camera is equipped with a macro lens (Canon EF 100 mm f/2.8 USM) and set up for fixed 1:1 magnification. Its optical axis is aligned with the optical axis of the collimating lens. The camera is mounted on a linear translation stage so that it can be moved along its optical axis in order to focus onto objects at different distances from the camera lens.

The experiment is performed in a dark room. The camera shutter time is set to 1 second and the shutter is triggered manually just before firing the ablation laser. The lasers are synchronized with a pulse generator connected to a PC allowing variation of the delay between the ablation and illumination laser emission.

## 2 OPTICAL SYSTEM ANALYSIS

A simplified paraxial ray analysis (Fig. 2) of the optical set-up gives an insight into image formation in this configuration and enables formulation of guidelines for setting up the imaging system. In the simplest approximation the set-up consists of two point illumination sources representing the fiber tips, two thin

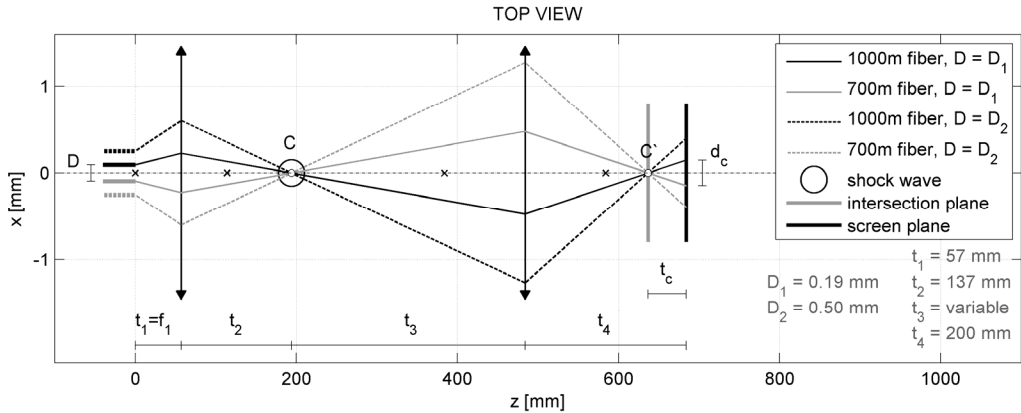


Fig. 2. Paraxial ray tracing analysis of the optical set-up. Solid and dashed lines represent ray traces that correspond to two different distances  $D$  between the fibers

converging lenses, a screen plane, representing the imaging sensor, and a spherically symmetric refractive object (SRO), representing the shock wave. The assumption of spherical symmetry is substantiated by the fact that we examine shock WFs at distances which are quite larger than the characteristic dimension of the interaction area (diameter of the ablation laser beam).

Thick lines on the left in Fig. 2 represent fiber tips: the dark and the light one represent the 1000 m and the 700 m fiber, respectively. Their right ends represent the point illumination sources. Thin lines represent rays emanating from the corresponding sources. Solid and dashed lines represent ray traces for two different distances between the sources. The thick solid circle represents the SRO.

From each point source only one ray is traced through the set-up – the ray which goes through the center of the SRO. These rays are not deflected by the SRO and determine the position of the symmetry centers of the SRO images displayed on the screen.

The ray traces in Fig. 2 that pass through the SRO center meet in a single point behind the imaging lens. If the screen is placed at this point then the SRO images projected by different illumination sources are concentric regardless of the distance  $D$  between the illumination sources (compare dashed and solid raytraces). Otherwise centers of symmetry of the SRO images do not coincide. We define the distance  $d_c$  between the centers of symmetry as eccentricity. Positive/negative  $d_c$  means that the centers lie on the same/opposite side of the optical axis as the corresponding light sources. Fig. 3 shows the

dependence of eccentricity  $d_c$  on the distance  $t_3$  which is variable in our case, while  $t_4$  is fixed by setting the optical magnification. The solid line represents the prediction of the paraxial model and the symbols represent the actually measured data. Fig. 4 shows 3 images which were used to determine the 3 indicated symbols (a, b, c) in Fig. 3. The actual procedure used to determine the measured data from the acquired images is described in the next section. Fig. 3 (arrow a) clearly shows that it is possible to set-up the optical system in such a way that the acquired images exhibit concentric WFs. In practice this is achieved by focusing the imaging system on the shock wave center. It is of practical interest to note that eccentricity  $d_c$  is independent of the distances  $t_1 = f_1$  and  $t_2$ . Paraxial ray analysis assuming thick lenses has also been performed and revealed essentially the same results about dependence of the eccentricity  $d_c$  on the distance  $t_3$ .

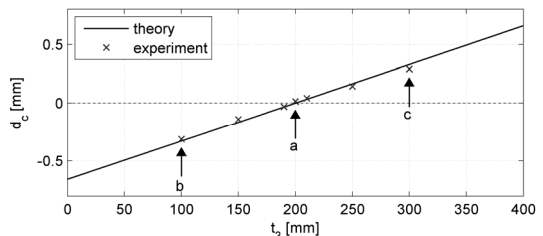


Fig. 3. Eccentricity  $d_c$  as a function of the distance  $t_3$  between the shock wave center and the imaging lens; data points marked by a, b, and c have been determined from images in Fig. 4

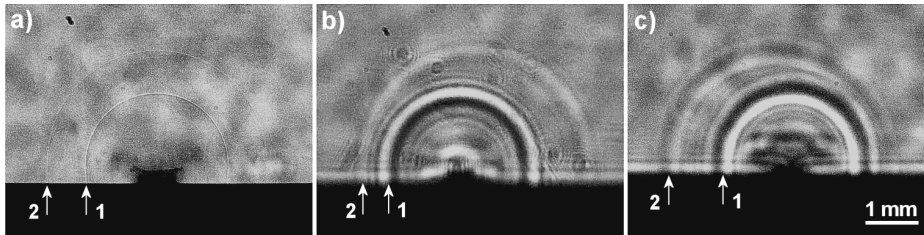


Fig. 4. Shock wave images acquired in three different camera positions indicated in Fig. 3; arrows 1 and 2 mark shock WFs illuminated by flashes from the 700 and 1000 m fibers, respectively

### 3 RESULTS AND DISCUSSION

Fig. 4 shows images acquired by the described set-up at three different distances  $t_3$  between the shock wave center and the imaging lens. The dark lower part of the images represents water, the brighter upper part air. Fig. 4a shows the image acquired when the camera was focused onto the shock wave center. Images in Figs. 4b and c were taken with camera focused on points 100 mm nearer and further from the center, respectively. The shock WFs (indicated by the arrows) clearly exhibit circular symmetry which is an evidence that the assumption of spherical symmetry of the SRO in the above analysis is essentially correct. The two WFs in Fig. 4a are nearly concentric while in Figs. 4b and c they exhibit eccentricity of similar magnitude and opposite sign. Eccentricity  $d_c$  was calculated by extracting the points that lie on each WF, fitting general circles to these points using a least squares algorithm and determine distances between the circle centers obtained by the fit. The obtained eccentricity data points are shown in Fig. 3.

By focusing the camera onto the shock wave center we acquire images with very thin WFs and rather poor contrast, so that the weaker second WF may be lost in the noisy image background. By focusing the camera off the shock wave center we obtain a bit blurred WF images with a better contrast. In practice, therefore, it may prove better for subsequent image analysis to focus the camera slightly off the shock wave center.

To demonstrate application of the method we present in Fig. 5 six samples from a sequence of images, acquired by changing the time delay between the ablation and illumination laser pulses. The time delays of the two illumination laser pulses are indicated on each image. The

other conditions are as described above. The dark objects at the top and the right side of the images represent the output aperture of the ablation laser and an acoustic transducer, respectively. The acoustic transducer was used to acquire the time evolution of the shock wave. A comparison of the results obtained by the shadowgraph and acoustic detection will be the subject of another publication.

Two circular WFs are clearly visible in each image, representing the positions of the same shock in two time instants, determined by the illumination flashes from the two fibers. Careful inspection of the images reveals slight ellipticity of the WFs: in the early evolution phase (short delays) the major axis of the ellipse parallels water surface, while later it becomes perpendicular to it (e.g. Figs. 5a, b and c). This indicates a slight non-uniformity of shock expansion: the shock travels slightly faster in the direction perpendicular to the water surface than in the other directions. Ellipticity gradually vanishes in the later phase (e.g. Figs. 5d, e and f).

By examination and analysis of a sequence of images, acquired with different time delays, we obtain the trajectory of the expanding shock wave (Fig. 6). Shock radius is determined by extracting a WF using image analysis, assuming that the transition between the darkest and the brightest band of a WF represents its actual position at the moment of illumination. For the purpose of comparison with the theoretical data, a circle is fitted to the extracted WF points to determine the WF radius. The time delay is determined from the oscilloscope traces of signals from photodetectors, monitoring emission from the two lasers. Marker pairs of equal shape and color in Fig. 6 represent measured data obtained from the same image. The solid line represents the theoretical trajectory, obtained by fitting the numerical solution [13] of the point explosion

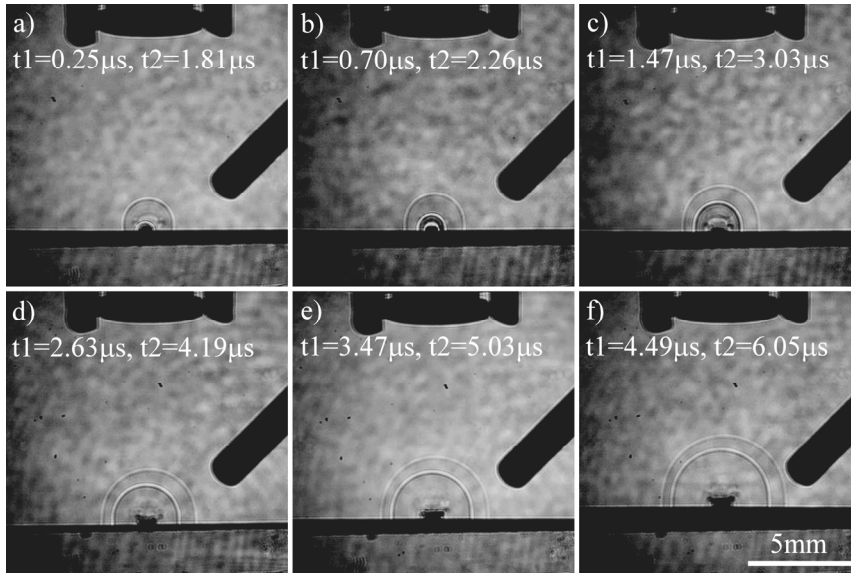


Fig. 5. Illustration of ablative shock wave evolution: images of 6 shock waves acquired by varying the time delay between the ablation and illumination laser pulses

model [14] to the measured data using blast energy as the fitting parameter. Comparing theoretical and experimental data we observe slight systematic misfit in the early phase which arises from the ellipticity discussed above. As evident from Fig. 6, the method enables obtaining a reasonable shock trajectory estimate using only a few acquired images. Assuming that the energy contained in a hemispherical wave is half of the blast energy that would produce the same mechanical effect in the spherical case we find from data in Fig. 6 that about 10% of the incident Er:YAG energy is contained within the shock wave propagated in air in this particular case.

Fig. 7 illustrates the application of the method for studying complex shock waves

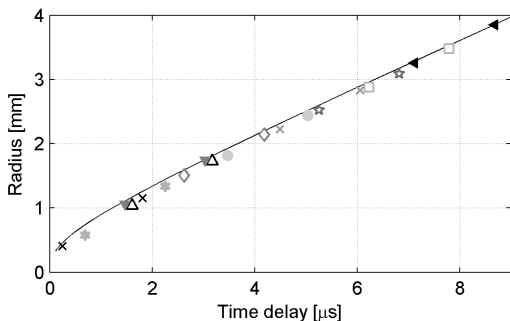


Fig. 6. Shock wave trajectory; equal marker pairs represent data obtained from the same captured image; solid line represents fitted theoretical spherical shock wave trajectory

generated during interaction of free-running Er:YAG laser pulses with water surface. Short spikes within a free-running pulse may possess enough energy to generate a sequence of shock waves [3] and [4]. In the experiment of Fig. 7 we use 10 µs Er:YAG pulses with spikes that generate three distinct shock WFs (A, B and C).

Comparing on the same image the respective WF positions in two time instances gives an insight into their propagation and the evolution of the whole wavefield. Some eccentricity  $d_e$  in such cases is useful as it facilitates distinction between the WFs acquired in two moments of time.

The method could be modified to allow acquisition an expanding shock wave in more than two time instances on a single image by

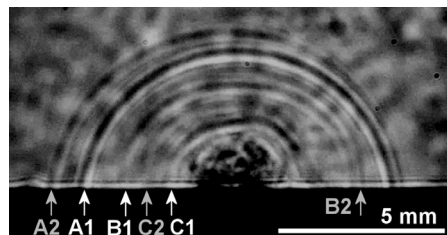


Fig. 7. Visualization of complex shock waves resulting from multiple spikes during one Er:YAG laser pulse; A1, B1, and C1 represent shock WFs illuminated by the 700 m fiber flash; A2, B2 and C2 represent the same shock WFs illuminated by the 1000 m fiber flash

using more than two fibers of different length, all aligned in a single row. The method is also applicable to studies of shock waves and related phenomena within transparent media (well away from any boundaries), e.g. for the studies of laser induced breakdown in liquids [15] and [16]. Because of greater shock wave speed in dense liquids the delay between two illumination instances should be relatively shorter.

#### 4 CONCLUSION

The double-exposure shadowgraph method, described in this paper, allows imaging of the same shock wave in two time instances. A single image thus gives insight into shock wave propagation and evolution. The shock wave is illuminated by pulsed green laser light coupled into two optical fibers of different lengths. The method has been applied to study spherical shock waves generated in air during interaction of Er:YAG laser light with water surface. By properly adjusting the set-up it is possible to examine propagation of multiple shock WFs using a single image.

#### 5 REFERENCES

- [1] Steiner, R. (2008). Medical applications of mid-ir solid-state lasers. *Mid-Infrared Coherent Sources and Applications*. Springer Netherlands, p. 575-588.
- [2] Niemz, M.H. (2002). *Laser-Tissue Interactions: Fundamentals and Applications*. 2<sup>nd</sup> ed. Springer-Verlag, Berlin, Heidelberg.
- [3] Nahen, K., Vogel, A. (1999). Investigations on acoustic on-line monitoring of IR laser ablation of burned skin. *Lasers in Surgery and Medicine*, vol. 25, no. 1, p. 69-78.
- [4] Grad, L., Možina, J. (1996). Optodynamic studies of Er:YAG laser induced microexplosions in dentin. *Applied Surface Science*, vol. 96, p. 591-595.
- [5] Nahen, K., Vogel, A. (2002). Plume dynamics and shielding by the ablation plume during Er:YAG laser ablation. *Journal of Biomedical Optics*, vol. 7, no. 2, p. 165-178.
- [6] Settles, G.S. (2001). *Schlieren and shadowgraph techniques*. Springer-Verlag, Berlin.
- [7] Diaci, J. (1992). Response functions for the laser beam deflection probe for detection of spherical acoustic waves. *Review of Scientific Instruments*, vol. 63, p. 5306-5310.
- [8] Villagran-Muniz, M., Sobral, H., Camps, E. (2001). Shadowgraphy and interferometry using a CW laser and a CCD of a laser-induced plasma in atmospheric air. *IEEE Transactions on Plasma Science*, vol. 29, no. 4, p. 613-616.
- [9] Požar, T., Možina, J. (2009). Homodyne quadrature laser interferometer applied for the studies of optodynamic wave propagation in a rod. *Strojniški vestnik – Journal of Mechanical Engineering*, vol. 55, no. 10, p. 575-580.
- [10] Amer, E., Gren, P., Sjudahl, M. (2008). Shock wave generation in laser ablation studied using pulsed digital holographic interferometry. *Journal of Physics D: Applied Physics*, vol. 41, p. 215502.
- [11] Diaci, J., Možina, J. (1995). Multiple-pass laser beam deflection probe for detection of acoustic and weak shock waves in fluids. *Review of Scientific Instruments*, vol. 66, p. 4644-4648.
- [12] Diaci, J., Hurley, D., Wagner, J., Možina, J. (1996). Simultaneous monitoring of ablative shocks in air by high-speed cineholography and multiple-pass beam deflection probe. *Applied Surface Science*, vol. 96-98, p. 154-158.
- [13] Goldstine, H.H., Von Neumann, J. (1955). Blast wave calculation. *Communications on Pure and Applied Mathematics*, vol. 8, no. 2, p. 327-353.
- [14] Kandula, M., Freeman, R. (2008). On the interaction and coalescence of spherical blast waves. *Shock Waves*, vol. 18, p. 21-33.
- [15] Petkovšek, R., Možina, J., Močnik, G. (2005). Optodynamic characterization of shock waves after laser-induced breakdown in water. *Optics Express*, vol. 13, no. 11, p. 4107-4112.
- [16] Gregorčič, P., Petkovšek, R., Možina, J. (2007). Investigation of a cavitation bubble between a rigid boundary and a free surface. *Journal of Applied Physics*, vol. 102, no. 9, p. 094904.